Clinical and Hemodynamic Features of Aneurysm Rupture in Coil Embolization of Intracranial Aneurysms

Tomoaki Suzuki *, Hitoshi Hasegawa, Kohei Shibuya, Hidemoto Fujiwara, Makoto Oishi

Posted Date: 13 May 2024

doi: 10.20944/preprints202405.0408.v1

Keywords: intraprocedural rupture; cerebral aneurysm; coil embolization; computational fluid dynamics; flow impingement zone; pressure; wall shear stress

 doi:10.20944/preprints202405.0408.v1

Article

Clinical and Hemodynamic Features of Aneurysm Rupture in Coil Embolization of Intracranial Aneurysms

Tomoaki Suzuki *, Hitoshi Hasegawa, Kohei Shibuya, Hidemoto Fujiwara, Makoto Oishi

Department of Neurosurgery, Brain Research Institute, Niigata University, 1-757 Asahimachi-Dori, Niigata 951-8585, Japan; e-mail@e-mail.com

* Correspondence: t.suzuki2078@gmail.com

Abstract: Intraprocedural rupture (IPR) is a severe complication of coil embolization (CE) for intracranial aneurysms, yet the clinical and hemodynamic features of rupture risk areas remain unclear. From January 2013 to December 2023, 435 saccular cerebral aneurysms (316 unruptured, 119 ruptured) underwent CE at our institution. Included were cases where extravasation or coil protrusion occurred during CE. The rupture point was determined from postoperative data, and computational fluid dynamics (CFD) analysis was conducted to assess hemodynamic features. IPR occurred in six aneurysms (1.3%; three ruptured, three unruptured; dome size: 4.7±1.8 mm, D/N: 1.5±0.5, locations: four internal carotid artery [ICA], one anterior cerebral artery, one middle cerebral artery). ICA aneurysms were treated using adjunctive techniques (three balloon-assisted, one stent-assisted). Two aneurysms (M1M2 and A1) were treated simply, yet had relatively small and misaligned domes. CFD analysis identified the rupture point as a flow impingement zone with maximum pressure (Pmax) in five aneurysms (83.3%). Time-averaged wall shear stress (WSS) was locally reduced around this area (1.3±0.7 [Pa]). Hemodynamically unstable areas indicated fragile, thin walls with rupture risk. Microcatheter insertion along the inflow zone, directed towards the caution area, was practiced. The presence of a flow impingement zone with Pmax and low WSS suggests potential aneurysm rupture in CE, particularly with adjunctive techniques. Small aneurysms, especially those with axial misalignment, warrant careful consideration due to the risk of excessive flow impact stress on the aneurysm wall.

Keywords: intraprocedural rupture; cerebral aneurysm; coil embolization; computational fluid dynamics; flow impingement zone; pressure; wall shear stress

1. Introduction

The rupture of cerebral aneurysms induces life-threatening subarachnoid hemorrhage (SAH), a devastating cerebrovascular condition. While microsurgical clipping has long been a standard treatment for intracranial aneurysms, the endovascular approach has emerged as a crucial option for averting aneurysm rupture. Endovascular surgery is widely employed in treating cerebral aneurysms. Coil embolization, a less invasive alternative to surgical intervention, has demonstrated proven long-term efficacy in preventing aneurysm rupture [1–4]. Recent innovations in endovascular devices, including flow diverter stents, offer effective solutions for managing challenging aneurysms. Nonetheless, coil embolization remains essential to foster intra-aneurysmal thrombosis and mitigate the risk of delayed rupture. Despite the documented advances in endovascular technology such as microcatheters and coils, there remains a risk of subjecting the aneurysmal wall to mechanical stress during insertion. Careful manipulation of microcatheters and coils is imperative to prevent aneurysm wall rupture. Intra-procedural aneurysm rupture (IPR) stands as a devastating complication during coil embolization, with previous studies reporting occurrence rates ranging from approximately 1.4% to 7.7% [5–7], often resulting in periprocedural mortality or disability [8,9]. The vulnerability of the aneurysm wall to rupture stems from fragile thinning walls in unruptured aneurysms and the initial rupture point in ruptured ones [10], induced by abnormal hemodynamic stress [11]. Prior

 doi:10.20944/preprints202405.0408.v1

investigations have explored the hemodynamic characteristics of thinning walls in cerebral aneurysms, highlighting the role of abnormal hemodynamic stress, such as static pressure and wall shear stress, in precipitating unstable wall conditions [12,13]. Unlike surgical clipping, endovascular procedures entail inevitable challenges in visualizing the aneurysmal wall condition. Accurately predicting the localization of fragile walls is critical for averting fatal IPR, particularly during endovascular interventions. Although studies have examined hemodynamic changes in thinning walls during intraoperative observations [14,15], the hemodynamic features of areas at risk of rupture during endovascular treatment remain unexplored. This study seeks to elucidate the clinical and hemodynamic characteristics of IPR in the endovascular management of cerebral aneurysms.

2. Materials and Methods

2.1. Patients and Aneurysm Characteristics

From January 2012 to December 2023, 435 intracranial cerebral aneurysms (316 unruptured, 119 ruptured) underwent coil embolization at our hospital. We conducted a retrospective investigation on patients who experienced extravasation or coil protrusion from the aneurysm dome. The rupture point was identified, and Computational Fluid Dynamics (CFD) analysis was carried out to elucidate the hemodynamic features of that region. Table 1 presents the patients' characteristics of the IPR.

Table 1. Patient characteristics of IPR.

N=6	
Sex (female:male)	5:1
Mean age (years)	62.8±15.3
Aneurysm Size	
Dome size (mm)	4.7±1.8
Neck size (mm)	3.2±0.8
D/N	1.5±0.5
Aneurysm Location	
ICA	4
MCA	1
ACA	1
Treatment	
Simple coiling	2
Ballon assisted coiling	3
Stent assisted coiling	1

2.2. CFD Analysis

The CFD analysis utilized a commercial package, hemoscope (EBM Corp, Tokyo, Japan), specifically designed for analyzing cerebral aneurysm flow dynamics [16]. Further details on the analysis are provided below. Pressure and Wall Shear Stress (WSS) at the rupture site were evaluated. Results of the CFD analysis are outlined in Figures 1–4 and Table 2.

 doi:10.20944/preprints202405.0408.v1

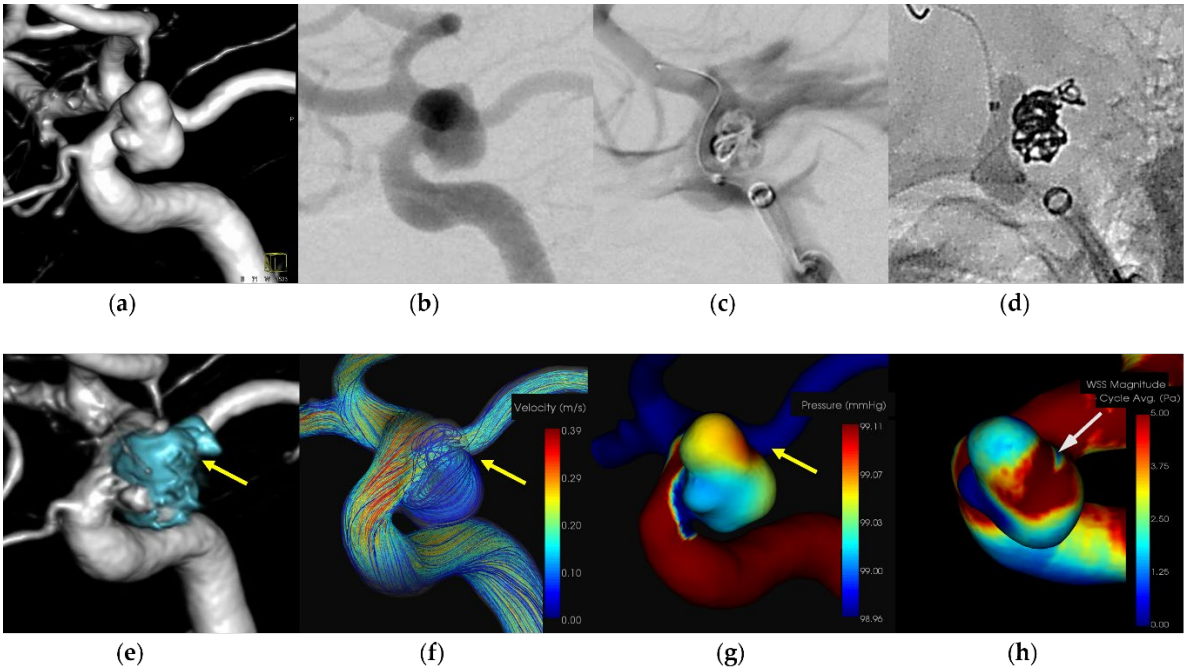

Figure 1. In case 1, an unruptured right internal carotid paraclinoid aneurysm (dome size: 6.5mm) was treated by balloon-assisted coiling. (a) Volume rendering (VR) image (pretreatment) (b) Digital subtraction angiography (DSA) image (pretreatment) (c) Extravasation after inserting the framing coil (d) Coil protrusion from intraprocedural rupture (IPR) site (yellow arrow) (e)VR image (posttreatment) and coil protrusion from IPR site (yellow arrow) (f) The IPR site corresponds to the flow impingement zone (yellow arrow) (g) The IPR site corresponds to the maximum pressure area (yellow arrow) (h) Wall shear stress decreased locally around the IPR site (white arrow: TAWSS 0.9 [Pa]).

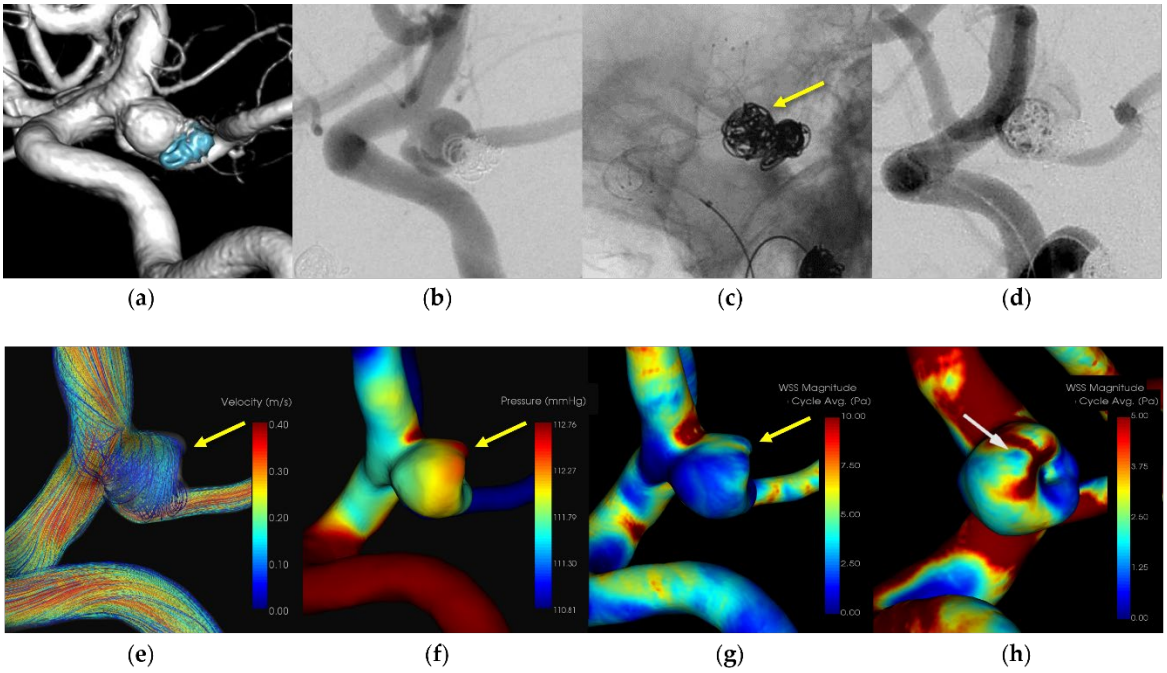

Figure 2. In case 2, an unruptured recurrent right internal carotid – posterior communicating artery aneurysm (dome size: 5.0mm) was treated by stent-assisted coiling. (a) Volume rendering (VR) image (pretreatment) (b) Digital subtraction angiography (DSA) image (pretreatment) (c) Stent-assisted coiling with LVIS and the head of the microcatheter (yellow arrow) (d) Extravasation after inserting

 doi:10.20944/preprints202405.0408.v1

the filling coil and the rupture point of the aneurysmal dome around the head of the microcatheter (e) The IPR site corresponds to the flow impingement zone (yellow arrow) (f)The IPR site corresponds to the maximum pressure area (yellow arrow) (g) Wall shear stress decreased locally around the IPR site (yellow arrow) (h) Localized low TAWSS around the IPR site is 1.5 [Pa] (white arrow).

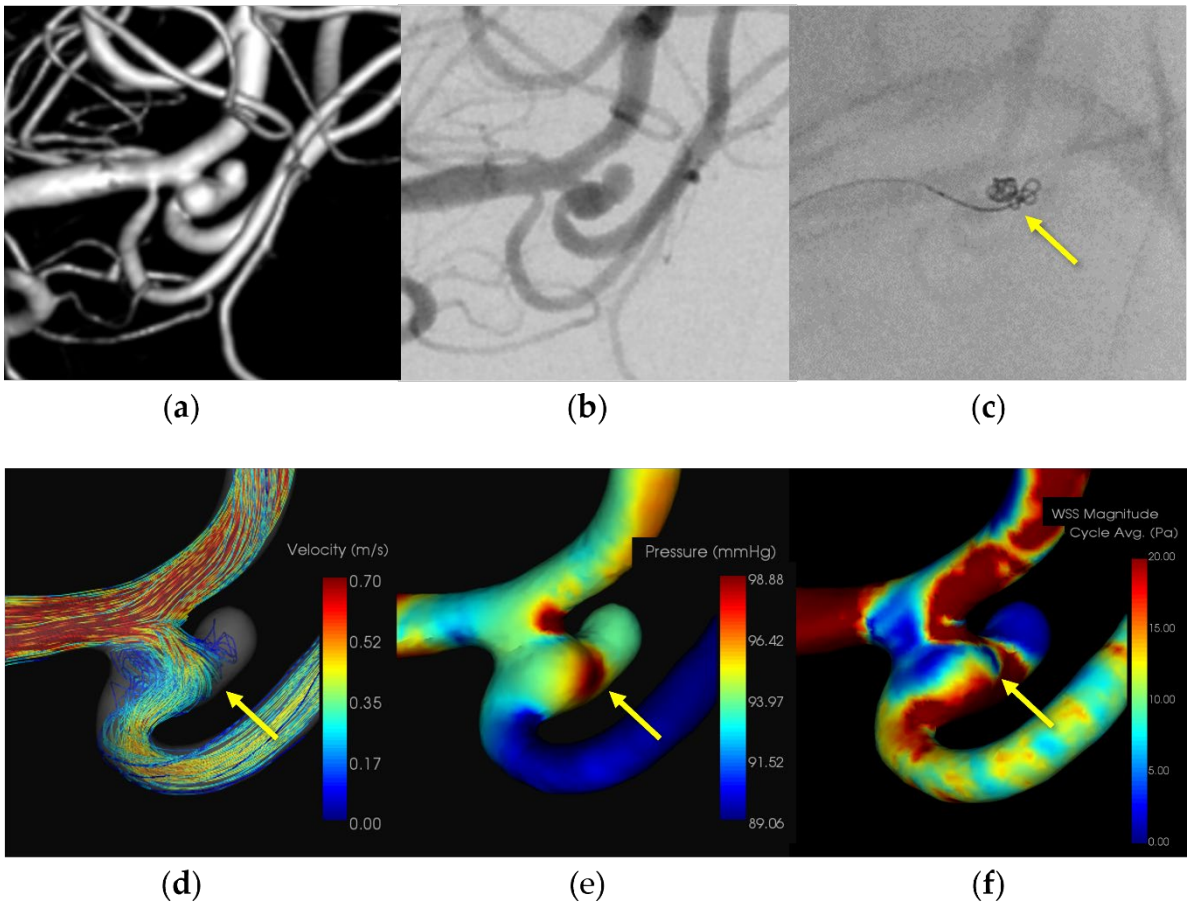

Figure 3. In case 3, a ruptured right middle cerebral artery aneurysm (dome size: 4.0mm) was treated by simple coiling. (a) Volume rendering (VR) image (pretreatment) (b) Digital subtraction angiography (DSA) image (pretreatment) (c) Coil protrusion from intraprocedural rupture (IPR) site (yellow arrow) (d) The IPR site corresponds to the flow impingement zone (yellow arrow) (e)The IPR site corresponds to the maximum pressure area (yellow arrow) (f) Wall shear stress decreased locally around the IPR site (yellow arrow: TAWSS 2.3 [Pa]).

Preprints.org (www.preprints.org) | NOT PEER-REVIEWED | Posted: 13 May 2024 doi:10.20944/preprints202405.0408.v1

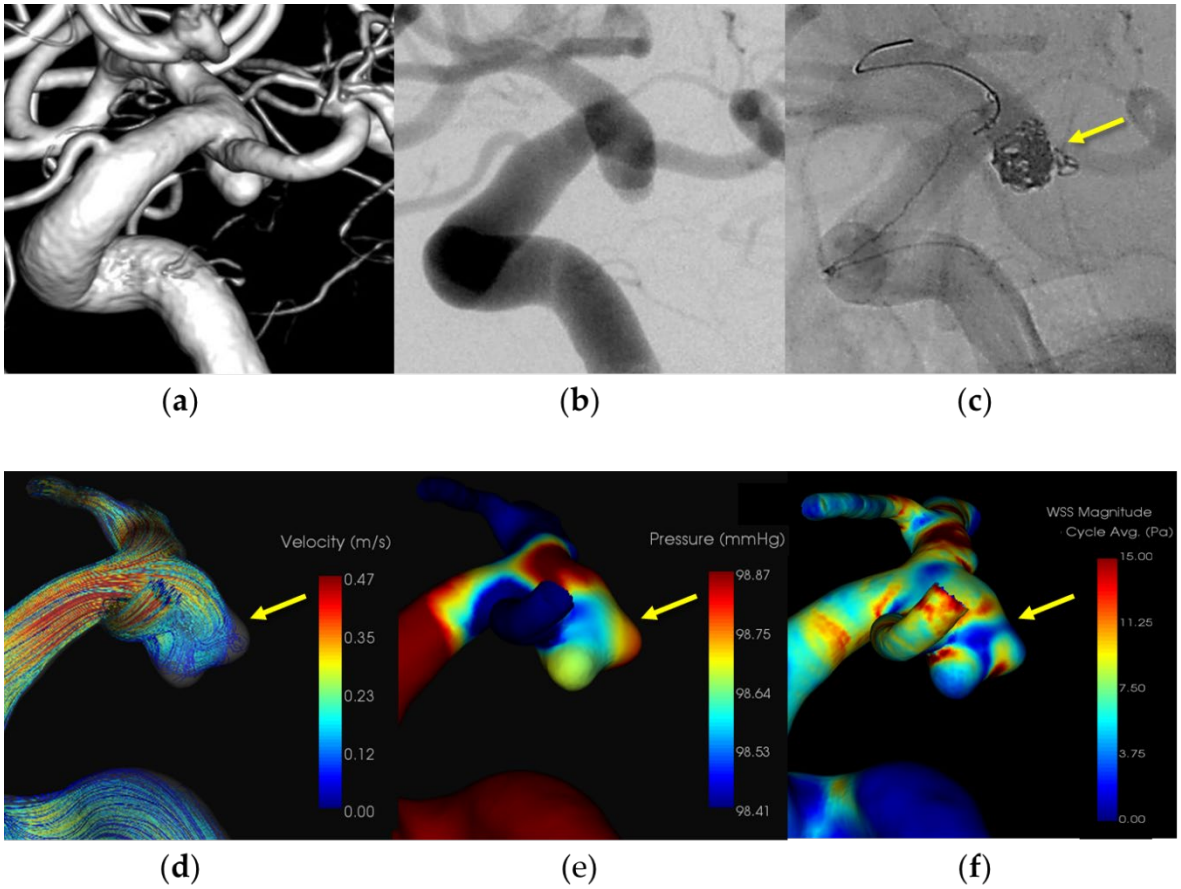

Figure 4. In case 4, a ruptured left internal carotid – posterior communicating artery aneurysm (dome size: 6.8 mm) was treated by balloon-assisted coiling. (a) Volume rendering (VR) image (pretreatment) (b) Digital subtraction angiography (DSA) image (pretreatment) (c) Coil protrusion from intraprocedural rupture (IPR) site (yellow arrow) (d) The IPR site corresponds to the flow impingement zone (yellow arrow) (e)The IPR site corresponds to the maximum pressure area (yellow arrow) (f) Wall shear stress decreased locally around the IPR site (yellow arrow: TAWSS 1.6 [Pa]).

Table 2. Hemodynamic characteristics of the patients with IPR.

Flow Impingement Zone = IPR Site	5/6 (83.3%)
Pressure	
IPR site (mmHg)	109.4±6.4
TAWSS	
IPR site (Pa)	1.3±0.7
Dome (Pa)	5.1±3.7

2.3. Pressure Elevation and Time-Averaged WSS (TAWSS) were Computed at the Aneurysmal Dome

For CFD analysis, vascular geometry was derived from Digital Imaging and Communications in Medicine (DICOM) data obtained from either CTA or 3D-DSA images and then reconstructed utilizing a medical image processing package (Ziostation2; Ziosoft, Inc., Japan). The current computation employed a pulsatile flow rate, with blood flow along the computational mesh processed using the Navier-Stokes equations. Blood properties were defined as those of an incompressible Newtonian fluid with a density of 1050 kg/m^3 and a dynamic viscosity of 0.004 Pa·s. Rigid walls for the blood vessels were assumed in the simulation. The total flow rate was determined based on the uniform wall shear stress hypothesis, with a constant WSS τ value set at 1.5 Pa.

 doi:10.20944/preprints202405.0408.v1

Boundary conditions were established following the constant wall shear stress theory, and the inlet and outlet vessel flow rates were calculated using the following equation:

$$Q = \frac{\tau\pi}{32\mu} D^3, \quad (1)$$

where Q, τ, μ, and D represent the flow rate, wall shear stress, fluid viscosity, and vascular diameter, respectively. This equation serves as a well-known theoretical basis for fully developed laminar pipe flow. Here, the wall shear stress was fixed at τ = 1.5 Pa. The inlet pressure was set to 100 mmHg, and the flow distribution at each outlet was determined in accordance with Murray's law.

A finite volume method was used to solve the governing equations unsteady Navier–Stokes equations and equation of continuity. The blood was assumed to be incompressible and Newtonian fluid, and the nature of the blood flow was allowed to have transient behaviors. The Euler method and second-order upwind scheme were adopted for discretizing the unsteady and convective acceleration terms. The convergent criteria were set at 10^{-4}.

To compare the baseline characteristics of the two groups, the unpaired two-sample t-test, were employed. A nominal P-value of .05 was utilized as the threshold indicating statistical significance. All statistical analyses were performed using GraphPad Prism version 7.02 (GraphPad Software, San Diego, CA, USA).

3. Results

During coil embolization, rupture occurred in 6 aneurysms, comprising 1.3% of cases. Among these, 3 aneurysms were ruptured, and 3 were unruptured, involving 4 internal carotid arteries (ICA), 1 anterior cerebral artery, and 1 middle cerebral artery (Table 1, Figure 1-3). All ICA aneurysms were treated with an adjunctive technique (three balloon-assisted and one stent-assisted technique), while the remaining two aneurysms (M1M2 and A1) were treated with a simple technique. Notably, the aneurysm dome in these cases was relatively small and axially misaligned from the bifurcation. The site of rupture was identifiable in five cases (83.3%), with a noted increase in pressure at a site consistent with the blood flow collision site (mean: 109±6.3 mmHg). During coil embolization, the microcatheter tip was positioned along the inflow zone and directed toward the flow impingement areas. Local decreasing wall shear stress was observed around the area (mean: 1.3±0.7 [Pa]) which was significantly lower than that of an aneurysmal dome (P<0.01). Table 2 presents the results of the CFD analysis.

3.1. Representative Cases

3.1.1. Case 1 (Figure 1)

A patient in her 40s with an unruptured right internal carotid artery aneurysm in the paraclinoid portion. The patient underwent treatment using a balloon-assisted technique under general anesthesia. An 8-Fr Roadmaster catheter (Goodman, Aichi, Japan) was utilized as a guiding catheter, while coil embolization was performed with a Phenom 17 microcatheter (Medtronic Neurovascular) coupled with a 072 Navien intermediate catheter. A SHOURYU HR (Kaneka Medics, Kanagawa, Japan) 4×7-mm balloon catheter was deployed at the aneurysmal neck for balloon-assisted coiling. Following the initial frame coiling without coil protrusion, contrast medium injection revealed extravasation. The balloon was then inflated to achieve hemostasis, resulting in the protrusion of an additional coil from the region around the microcatheter's head. Subsequent insertion of additional coils promptly halted the bleeding. The patient was discharged without any neurological deficits. CFD analysis indicated the location of the IPR at the coil protrusion site, suggesting pressure elevation due to flow impingement. Low WSS was localized around the rupture area.

3.1.2. Case 2 (Figure 2)

A patient in her 70s who had previously undergone coil embolization for an unruptured left internal carotid artery – posterior communicating artery aneurysm 12 years prior, underwent retreatment with stent-assisted coil embolization. A 7-Fr Emboy catheter (Codman Neuro, Raynham,

 doi:10.20944/preprints202405.0408.v1

MA) served as the guiding catheter in the internal carotid artery, while a RESTAR microcatheter (Medico's Hirata, Osaka, Japan) was positioned within the aneurysm. Stent placement was facilitated using a Headway 21 microcatheter (Terumo, Microvention, Japan). Coil embolization was performed following LVIS deployment (Microvention, Aliso Viejo, California, USA). Extravasation was observed during coil filling, originating from the rupture point of the aneurysmal dome around the microcatheter head. Immediate additional coil embolization effectively ceased the bleeding. The patient was discharged without any neurological deficits. CFD analysis pinpointed the extravasation site as the area of IPR, suggesting pressure elevation due to flow impingement. A localized low WSS was also identified around the rupture area.

3.1.3. Case 3 (Figure 3)

A patient in her 50s presented with a subarachnoid hemorrhage (Hunt and Kosnik grade 3) resulting from a ruptured left MCA M1-M2 bifurcation aneurysm, which was managed with coil embolization. An 8-Fr Roadmaster catheter (Goodman, Aichi, Japan) was positioned in the internal carotid artery as a guiding catheter, while coil embolization was conducted using a Phenom 17 microcatheter paired with a Cerulean DD6 intermediate catheter. During coil filling, protrusion of coils from the aneurysm dome and extravasation from the rupture point in the middle of the aneurysmal dome were observed. Immediate additional coil embolization successfully halted the bleeding. The patient was discharged without any neurological deficits. Subsequently, the patient was transferred to a rehabilitation hospital due to the initial damage caused by the subarachnoid hemorrhage. CFD analysis identified the location of the IPR at the site of extravasation, indicating pressure elevation with maximum pressure attributed to flow impingement. Additionally, there was a localized decrease in WSS in the ruptured area.

3.1.4. Case 4 (Figure 4)

A patient in her 70s with a subarachnoid hemorrhage (Hunt and Kosnik grade 3) resulting from a ruptured right internal carotid artery – posterior communicating artery aneurysm, which was managed with balloon-assisted coil embolization. An 8-Fr Roadmaster catheter (Goodman, Aichi, Japan) was positioned in the internal carotid artery as a guiding catheter, while coil embolization was conducted using an Excelsior SL-10 microcatheter (Boston Scientific, Natick, MA, USA) paired with a Cerulean DD6 intermediate catheter. A SHOURYU HR (Kaneka Medics, Kanagawa, Japan) 4×7-mm balloon catheter was deployed at the aneurysmal neck for balloon-assisted coiling. During coil filling, protrusion of coils from the aneurysm dome was observed. Immediate additional coil embolization successfully halted the bleeding. The patient was discharged without any neurological deficits. CFD analysis identified the location of the IPR at the site of extravasation, indicating pressure elevation with maximum pressure attributed to flow impingement. Additionally, there was a localized decrease in WSS in the ruptured area.

4. Discussion

IPR stands as a significant concern for endovascular surgeons, with undeniable implications for mortality and morbidity rates [17,18]. While the utilization of endovascular techniques has surged, along with the development of devices like coils, microcatheters, and stents for cerebral aneurysm treatment, the risk of IPR persists, even with meticulous manipulation. Unlike in open surgery, where thinning of the aneurysmal wall signals rupture susceptibility under passive mechanical stress from coils, the condition of the aneurysmal wall remains elusive during endovascular procedures. Findings from this investigation underscore that aneurysmal walls exhibiting hemodynamic features conducive to high pressure, such as in flow impingement zones, pose a heightened risk for IPR. In these zones, the microcatheter tends to navigate, and the inserted coil carries the potential to exert pressure on the vulnerable wall along the inflow angle. CFD emerges as a promising tool for identifying such vulnerable areas predisposing to IPR. This study represents the inaugural

 doi:10.20944/preprints202405.0408.v1

exploration of the hemodynamic characteristics associated with IPR during coil embolization of cerebral aneurysms.

Flow impingement at the aneurysmal walls, coupled with pressure elevation, has long been recognized as a significant risk factor in cerebral aneurysms, with the inflow pattern and high-velocity inflow jet being closely linked to hemodynamic instabilities [19,20]. In this study, we detected this hemodynamic feature at the intraoperative rupture point in the majority of IPR aneurysms (One ICA aneurysm showed no Pmax area at the rupture site; however, it was adjacent to the Pmax area). Previous CFD studies, in conjunction with operative observations during clipping, have revealed that areas of thinning walls exhibit the highest pressure with flow impingement in unruptured aneurysms [13,21]. Such hemodynamic stress is often concentrated in the aneurysmal wall surrounding the inflow zone, traversed by a microcatheter during coil embolization, indicating the possible presence of thinning and fragile aneurysmal walls in this region. Flow impingement, as described in prior CFD studies, is recognized as a hazardous hemodynamic feature predisposing to aneurysmal rupture [22,23]. Furthermore, excessive hemodynamic stress, accompanied by pressure elevation, is believed to initiate thinning and fragility in rupture-prone walls [24,25], potentially resulting in severe bleeding. WSS represents another critical hemodynamic stress factor strongly associated with aneurysm growth and rupture [26,27]. Particularly, low WSS has been robustly linked to aneurysm rupture, with previous research indicating its role in endothelial cell dysfunction and wall degeneration within aneurysms [28,29]. In our study, localized low WSS was observed around the IPR site, notably decreasing within the aneurysmal dome. These findings suggest that low WSS also contributes significantly to the hemodynamic stresses underlying IPR, possibly due to the presence of fragile aneurysm walls.

Mechanical stress induced by coils represents another significant factor in IPR. This stress poses the risk of stiffness and friction within the aneurysmal wall, potentially leading to rupture during coil embolization, particularly in cases of small aneurysms or when the microcatheter exhibits reduced flexibility [30]. Two IPR cases (A1 and M2) were managed using a straightforward technique, with relatively small dome sizes and axial misalignment from the bifurcation, possibly resulting in microcatheter fixation. Morphologically, small aneurysms have been identified as a risk factor for IPR [31]. Adjunctive techniques such as balloon- and stent-assisted procedures hold the potential to induce IPR due to microcatheter fixation during coil insertion [32]. In our investigation, all four ICA IPR cases were treated with adjunctive techniques. Extravasation occurred during coil embolization, leading to a gradual loss of microcatheter mobility. The trajectory of the microcatheter followed the inflow streamline into the aneurysm, culminating in an impingement zone at the intraoperative rupture site. The utilization of adjunctive techniques warrants cautious consideration due to the risk of excessive stress on the aneurysm wall, particularly within the flow impingement zone where the wall may be particularly fragile.

A combination of CFD analysis for IPR revealed that the lower flexibility of the microcatheter could increase mechanical stress during coil insertion in the flow impingement zone, leading to pressure elevation and low WSS, indicating potential fragile thinning or ruptured walls. Notably, no prior studies have explored CFD analysis of IPR in cerebral aneurysms.

While endovascular treatment has increasingly adopted a flow-diversion strategy, coil embolization remains indispensable for preventing aneurysm rupture. Unlike microsurgical clipping, endovascular surgeons lack direct visibility of the aneurysmal wall condition, necessitating caution regarding contact during the procedure. Our findings may serve as a foundation for employing CFD analysis to mitigate catastrophic IPR occurrences.

4.1. Limitations

This study encountered several limitations. Firstly, the analysis was restricted by the small number of cases examined. Consequently, further investigations employing larger sample sizes are warranted to validate the findings. Secondly, the CFD analysis lacked patient-specific boundary conditions, which could be established through magnetic resonance and echo imaging, where available. Thirdly, while previous CFD studies have suggested that the area of flow impingement

 doi:10.20944/preprints202405.0408.v1

may indicate aneurysmal thinning or a ruptured wall, this aspect has not been evaluated in open surgery settings.

5. Conclusion

Previous reports have indicated that the aneurysm wall is prone to thinning at sites of pressure elevation resulting from blood flow collision. Given the similar hemodynamic characteristics observed at the rupture site in our study, the risk of rupture may have been elevated. Utilizing a hemoscope to predict regions at risk of rupture based on our findings could serve as a valuable clinical support tool for mitigating potentially fatal risks.

Author Contributions: Conceptualization, TS; methodology, TS; software, TS; validation, TS.; formal analysis, TS; investigation, TS; data curation, TS.; writing—original draft preparation, TS; writing—review and editing, TS; visualization, TS; supervision, HH, KS, HF, MO. All authors have read and agreed to the published version of the manuscript.

Funding: None.

Institutional Review Board Statement: This study was approved by the ethics committee of our hospital (approval number: 2020-0027).

Informed Consent Statement: Patient consent was waived due to no identifiable private information included in the article.

Data Availability Statement: The original contributions presented in the study are included in the article, further inquiries can be directed to the corresponding author.

Conflicts of Interest: None.

References

1. Spetzler, R.F.; McDougall, C.G.; Zabramski, J.M.; Albuquerque, F.C.; Hills, N.K.; Nakaji, P.; Karis, J.P.; Wallace, R.C. Ten-year analysis of saccular aneurysms in the Barrow Ruptured Aneurysm Trial. *J Neurosurg* **2019**, *132*, 771–776. DOI:10.3171/2018.8.JNS181846.
2. Luther, E.; McCarthy, D.J.; Brunet, M.C.; Sur, S.; Chen, S.H.; Sheinberg, D.; Hasan, D.; Jabbour, P.; Yavagal, D.R.; Peterson, E.C.; et al. Treatment and diagnosis of cerebral aneurysms in the post-International Subarachnoid Aneurysm Trial (ISAT) era: trends and outcomes. *J Neurointerv Surg* **2020**, *12*, 682–687. DOI:10.1136/neurintsurg-2019-015418.
3. Calvanese, F.; Auricchio, A.M.; Pohjola, A.; Hafez, A.; Nurminen, V.; Korja, M.; Numminen, J.; Lehecka, M.; Raj, R.; Niemelä, M. Changes in treatment of intracranial aneurysms during the last decade in a large European neurovascular center.. *Acta Neurochir (Wien)* **2024**, *166*, 173. DOI:10.1007/s00701-024-06064-4.
4. Salem, M.M.; Maragkos, G.A.; Gomez-Paz, S.; Ascanio, L.C.; Ngo, L.H.; Ogilvy, C.S.; Thomas, A.J.; Moore, J.M. Trends of ruptured and unruptured aneurysms treatment in the United States in post-ISAT era: A national inpatient sample analysis. *J Am Heart Assoc* **2021**, *10*, e016998. DOI:10.1161/JAHA.120.016998.
5. Stapleton, C.J.; Walcott, B.P.; Butler, W.E.; Ogilvy, C.S. Neurological outcomes following intraprocedural rerupture during coil embolization of ruptured intracranial aneurysms. *J Neurosurg* **2015**, *122*, 128–135. DOI:10.3171/2014.9.JNS14616.
6. Park, Y.K.; Yi, H.J.; Choi, K.S.; Lee, Y.J.; Chun, H.J. Intraprocedural rupture during endovascular treatment of intracranial aneurysm: clinical results and literature review. *World Neurosurg* **2018**, *114*, e605–e615. DOI:10.1016/j.wneu.2018.03.040.
7. Kawabata, S.; Imamura, H.; Adachi, H.; Tani, S.; Tokunaga, S.; Funatsu, T.; Suzuki, K.; Sakai, N. Risk factors for and outcomes of intraprocedural rupture during endovascular treatment of unruptured intracranial aneurysms. *J Neurointerv Surg* **2018**, *10*, 362–366. DOI:10.1136/neurintsurg-2017-013156.
8. Cloft, H.J.; Kallmes, D.F. Cerebral aneurysm perforations complicating therapy with Guglielmi detachable coils: a meta-analysis. *AJNR Am J Neuroradiol* **2002**, *23*, 1706–1709.
9. Elijovich, L.; Higashida, R.T.; Lawton, M.T.; Duckwiler, G.; Giannotta, S.; Johnston, S.C.; Cerebral Aneurysm Rerupture After Treatment (CARAT) Investigators. Predictors and outcomes of intraprocedural rupture in patients treated for ruptured intracranial aneurysms: the CARAT study. *Stroke* **2008**, *39*, 1501–1506. DOI:10.1161/STROKEAHA.107.504670.
10. Chen, X.L.; Chen, Y.; Ma, L.; Burkhardt, J.K.; Wardell, T.; Wang, C.; Guo, G.; Wang, S.; Zhao, Y.L. Translucent appearance of middle cerebral artery bifurcation aneurysms is risk factor for intraoperative aneurysm rupture during clipping. *World Neurosurg* **2017**, *101*, 149–154. DOI:10.1016/j.wneu.2017.01.097.

11. Frösen, J.; Cebral, J.; Robertson, A.M.; Aoki, T. Flow-induced, inflammation-mediated arterial wall remodeling in the formation and progression of intracranial aneurysms. *Neurosurg Focus* **2019**, *47*, E21. DOI:10.3171/2019.5.FOCUS19234.
12. Kadasi, L.M.; Dent, W.C.; Malek, A.M. Colocalization of thin-walled dome regions with low hemodynamic wall shear stress in unruptured cerebral aneurysms. *J Neurosurg* **2013**, *119*, 172–179. DOI:10.3171/2013.2.JNS12968.
13. Suzuki, T.; Takao, H.; Suzuki, T.; Kambayashi, Y.; Watanabe, M.; Sakamoto, H.; Kan, I.; Nishimura, K.; Kaku, S.; Ishibashi, T.; et al. Determining the presence of thin-walled regions at high-pressure areas in unruptured cerebral aneurysms by using computational fluid dynamics. *Neurosurgery* **2016**, *79*, 589–595. DOI:10.1227/NEU.0000000000001232.
14. Fan, X.X.; Geng, J.W.; He, C.; Hu, P.; Sun, L.Y.; Zhang, H.Q. Analysis of the wall thickness of intracranial aneurysms: can computational fluid dynamics detect the translucent areas of saccular intracranial aneurysms and predict the rupture risk preoperatively? *Front Neurol* **2022**, *13*, 1075078. DOI:10.3389/fneur.2022.1075078.
15. Veeturi, S.S.; Patel, T.R.; Baig, A.A.; Chien, A.; Monteiro, A.; Waqas, M.; Snyder, K.V.; Siddiqui, A.H.; Tutino, V.M. Hemodynamic analysis shows high wall shear stress is associated with intraoperatively observed thin wall regions of intracranial aneurysms. *J Cardiovasc Dev Dis* 2022, 9. DOI:10.3390/jcdd9120424.
16. Sugiyama, S.I.; Niizuma, K.; Sato, K.; Rashad, S.; Kohama, M.; Endo, H.; Endo, T.; Matsumoto, Y.; Ohta, M.; Tominaga, T. Blood flow into basilar tip aneurysms: A predictor for recanalization after coil embolization. *Stroke* **2016**, *47*, 2541–2547. DOI:10.1161/STROKEAHA.116.013555.
17. Elijovich, L.; Higashida, R.T.; Lawton, M.T.; Duckwiler, G.; Giannotta, S.; Johnston, S.C. Predictors and outcomes of intraprocedural rupture in patients treated for ruptured intracranial aneurysms: the CARAT study. *Stroke* **2008**, 39, 1501–1506.
18. Yamagami, K.; Hatano, T.; Nakahara, I.; Ishii, A.; Ando, M.; Chihara, H.; Ogura, T.; Suzuki, K.; Kondo, D.; Kamata, T.; et al. Long-term outcomes after intraprocedural aneurysm rupture during coil embolization of unruptured intracranial aneurysms. *World Neurosurg* **2020**, *134*, e289–e297. DOI:10.1016/j.wneu.2019.10.038. (Epub 2019 Oct 16).
19. Mo, X.; Meng, Q.; Yang, X.; Li, H. The impact of inflow angle on aneurysm hemodynamics: A simulation study based on patient-specific intracranial aneurysm models. *Front Neurol* **2020**, *11*, 534096. DOI:10.3389/fneur.2020.534096.
20. Guo, H.; Yang, S.T.; Wang, J.W.; Li, H.; Gao, B.L.; Li, C.H. High hemodynamic stresses induce aneurysms at internal carotid artery bends. *Med (Baltim)* **2023**, *102*, e34587. DOI:10.1097/MD.0000000000034587.
21. Murayama, Y.; Fujimura, S.; Suzuki, T.; Takao, H. Computational fluid dynamics as a risk assessment tool for aneurysm rupture. *Neurosurg Focus* **2019**, *47*, E12. DOI:10.3171/2019.4.FOCUS19189.
22. Cebral, J.R.; Detmer, F.; Chung, B.J.; Choque-Velasquez, J.; Rezai, B.; Lehto, H.; Tulamo, R.; Hernesniemi, J.; Niemela, M.; Yu, A.; et al. Local hemodynamic conditions associated with focal changes in the intracranial aneurysm wall. *AJNR Am J Neuroradiol* **2019**, *40*, 510–516. DOI:10.3174/ajnr.A5970.
23. Omodaka, S.; Sugiyama, S.I.; Inoue, T.; Funamoto, K.; Fujimura, M.; Shimizu, H.; Hayase, T.; Takahashi, A.; Tominaga, T. Local hemodynamics at the rupture point of cerebral aneurysms determined by computational fluid dynamics analysis. *Cerebrovasc Dis* 2012, 34, 121–129. DOI:10.1159/000339678.
24. Jiang, P.; Liu, Q.; Wu, J.; Chen, X.; Li, M.; Li, Z.; Yang, S.; Guo, R.; Gao, B.; Cao, Y.; et al. Hemodynamic characteristics associated with thinner regions of intracranial aneurysm wall. *J Clin Neurosci* **2019**, *67*, 185–190. DOI:10.1016/j.jocn.2019.06.024. (Epub 2019 Jun 26).
25. Suzuki, T.; Stapleton, C.J.; Koch, M.J.; Tanaka, K.; Fujimura, S.; Suzuki, T.; Yanagisawa, T.; Yamamoto, M.; Fujii, Y.; Murayama, Y.; et al. Decreased wall shear stress at high-pressure areas predicts the rupture point in ruptured intracranial aneurysms. *J Neurol Surg* **2019**, 1–7.
26. Meng, H.; Tutino, V.M.; Xiang, J.; Siddiqui, A. High WSS or low WSS? Complex interactions of hemodynamics with intracranial aneurysm initiation, growth, and rupture: toward a unifying hypothesis. *AJNR Am J Neuroradiol* **2014**, *35*, 1254–1262. DOI:10.3174/ajnr.A3558. (Epub 2013 Apr 18).
27. Nordahl, E.R.; Uthamaraj, S.; Dennis, K.D.; Sejkorová, A.; Hejčl, A.; Hron, J.; Švihlová, H.; Carlson, K.D.; Suzen, Y.B.; Dragomir-Daescu, D. Morphological and hemodynamic changes during cerebral aneurysm growth. *Brain Sci* **2021**, *11*, 520. DOI:10.3390/brainsci11040520.
28. Sejkorová, A.; Dennis, K.D.; Švihlová, H.; Petr, O.; Lanzino, G.; Hejčl, A.; Dragomir-Daescu, D. Hemodynamic changes in a middle cerebral artery aneurysm at follow-up times before and after its rupture: a case report and a review of the literature. *Neurosurg Rev* **2017**, *40*, 329–338. DOI:10.1007/s10143-016-0795-7.
29. Zhang, Y.; Jing, L.; Zhang, Y.; Liu, J.; Yang, X. Low wall shear stress is associated with the rupture of intracranial aneurysm with known rupture point: case report and literature review. *BMC Neurol* **2016**, *16*, 231. DOI:10.1186/s12883-016-0759-0.

 doi:10.20944/preprints202405.0408.v1

30. Mitchell, P.J.; Muthusamy, S.; Dowling, R.; Yan, B. Does small aneurysm size predict intraoperative rupture during coiling in ruptured and unruptured aneurysms? *J Stroke Cerebrovasc Dis* **2013**, *22*, 1298–1303. DOI:10.1016/j.jstrokecerebrovasdis.2012.10.017.
31. Peng, F.; Feng, X.; He, X.; Niu, H.; Zhang, H.; Tong, X.; Zhang, B.; Xia, J.; Chen, X.; Xu, B.; et al. Independent predictors and risk score for intraprocedural rupture during endovascular treatment of small ruptured intracranial aneurysms (<5 mm). *Front Neurol* **2022**, *13*, 923645. DOI:10.3389/fneur.2022.923645.
32. Jiang, C.; Luan, D.; Wang, C.; Liu, Q.; Han, J.; Li, G. Risk and prognostic factors for rupture of intracranial aneurysms during endovascular embolization. *World Neurosurg* **2019**, *129*, e641–e649. DOI:10.1016/j.wneu.2019.05.233.